Spin transport in a unitary Fermi gas close to the BCS transition

M. P. Mink,* V. P. J. Jacobs, H. T. C. Stoof, and R. A. Duine
Institute for Theoretical Physics, Utrecht University, Leuvenlaan 4, 3584 CE Utrecht, Netherlands

Marco Polini
NEST, Istituto Nanoscienze-CNR and Scuola Normale Superiore, I-56126 Pisa, Italy

G. Vignale
Department of Physics and Astronomy, University of Missouri, Columbia, Missouri 65211, USA
(Received 21 August 2012; published 26 December 2012)

We consider spin transport in a two-component ultracold Fermi gas with attractive interspecies interactions close to the BCS pairing transition. In particular, we consider the spin-transport relaxation rate and the spin-diffusion constant. Upon approaching the transition, the scattering amplitude is enhanced by pairing fluctuations. However, as the system approaches the transition, the spectral weight for excitations close to the Fermi level is decreased by the formation of a pseudogap. To study the consequence of these two competing effects, we determine the spin-transport relaxation rate and the spin-diffusion constant using both a Boltzmann approach and a diagrammatic approach. The former ignores pseudogap physics and finite lifetime effects. In the latter, we incorporate the full pseudogap physics and lifetime effects, but we ignore vertex corrections, so that we effectively calculate single-particle relaxation rates instead of transport relaxation rates. We find that there is qualitative agreement between these two approaches, although the results for the transport coefficients differ quantitatively.

DOI: 10.1103/PhysRevA.86.063631 PACS number(s): 03.75.Ss, 05.30.Fk, 03.75.−b, 67.85.−d

I. INTRODUCTION

Over the last decade, there has been a growing interest in the physics community in the properties of spin transport, spurred by the idea of using the electron spin as a carrier of information. A spin current is a net flow of spin and is fundamentally different from a charge current because it relaxes in a different way. In particular, spin currents can be strongly affected by interactions, even in Galilean-invariant systems.

Ultracold fermion systems consisting of two spin species provide a valuable model system for the study of the effects of interactions on spin transport because of their high tunability and the absence of other factors which limit the spin conductivity, such as disorder. When the cloud of one species moves relative to the cloud of the other species, the latter is dragged along due to momentum relaxation by the interatomic interaction, and as a consequence, the spin current relaxes. This mechanism is called spin drag [1]. A similar phenomenon, Coulomb drag, occurs in bilayer systems, in which the drift momentum difference between the carriers in the top and bottom layers relaxes due to the Coulomb interaction [2,3].

In an important recent experimental study, the spin susceptibility, the spin-diffusion constant, and the relaxation rate of spin transport were investigated in a ultracold two-component fermion gas in the unitarity regime, where the interspecies scattering length goes to infinity so that the interactions are as strong as quantum mechanics allows [4,5]. Inspired by this work, the spin-transport relaxation rate and the spin-diffusion constant were calculated using a Boltzmann approach for high- and low-temperature ranges separately [6]. We also note the recent experimental work on the dynamic spin response in these gases by Hoinka *et al.* [7].

When an ultracold Fermi gas with two spin species and an attractive interaction between the spins is cooled to low enough temperatures, it shows a transition to a superfluid state, where the opposite-spin atoms pair up to form Cooper pairs. The effect of interactions on spin transport close to this BCS pairing transition is an interesting subject since two effects are competing. On the one hand, the scattering amplitude between fermions is enhanced by pairing fluctuations (preformed Cooper pairs) not taken into account in Ref. [6]. When the temperature is lowered, this effect ultimately leads to a diverging interaction strength and an instability in the system towards the BCS state at the critical temperature. As a consequence, transport coefficients such as the spin-transport relaxation rate and the spin-diffusion constant are expected to be strongly affected when the system approaches the transition. These effects were not seen experimentally in Ref. [4], possibly because T_c was not reached but possibly also due to the competing effect we discuss shortly.

In related work, for ultracold fermions with repulsive interactions, enhancement of the spin-transport relaxation rate was predicted close to the ferromagnetic transition [8] and for ultracold bosons close to Bose-Einstein condensation [9]. The latter was recently also observed experimentally [10]. Riedl *et al.* studied the frequencies and damping of collective modes in an ultracold Fermi gas close to the BCS pairing transition [11] and found an enhancement of the collision rate in a fermionic gas close to the BCS pairing transition. The behavior of the viscosity was studied in Ref. [12]. In electron-hole bilayers the electrons in one layer and holes in the other can form excitons, which are expected to condense for low enough temperatures. Theoretically, it was predicted that the transport

*m.p.mink@uu.nl

relaxation rate is enhanced when approaching this transition [13]. An enhancement was measured experimentally [14], although it is still under debate whether this enhancement was indeed caused by exciton condensation. Also, for a topological insulator thin film, an enhancement of the transport relaxation rate was predicted close to (in this case topological) exciton condensation [15].

However, as already mentioned, there is a competing effect at play. For temperatures below the transition temperature, the system is in the superfluid state, and the excitation spectrum is gapped. Already above T_c, a precursor of this gap can be seen as the suppression of spectral weight close to the Fermi level, a so-called pseudogap [16]. The suppressed spectral weight is closely linked to the reduced lifetime for these excitations. The effect of this pseudogap is to reduce the phase space for scattering events around the Fermi level, which is expected to reduce the enhancement of transport coefficients. We consider the competition between the increase in scattering amplitude due to pairing fluctuations on the one hand and the decrease in available phase space due to the pseudogap on the other and its effect on the transport relaxation rate and the spin-diffusion constant in this paper. For the spin susceptibility this competition was considered in Ref. [17], and we also note related work determining the static spin susceptibility for repulsive interactions in Ref. [18].

In general, the relaxation rate of a current and the decay rate of a single-particle excitation are different because of the amount the possible scattering directions contribute to either case. In the case of the decay of a single-particle excitation, all directions are weighed equally, but in the case of current relaxation, forward scattering (in the direction of the current) contributes much less than backscattering (in the direction opposite to the current). Theoretically, in diagrammatic calculations, a transport relaxation rate is obtained by inclusion of so-called vertex corrections to the appropriate response function. If these are neglected, the transport relaxation time is essentially equal to the single-particle relaxation time.

In this paper we consider a two-component gas of fermions consisting of two spin states labeled by $\sigma = \uparrow, \downarrow$. We consider the balanced case where the densities of each spin component are $n_\uparrow = n_\downarrow \equiv n$ and where both species have the dispersion $\xi(\boldsymbol{k}) = \hbar^2 k^2/2m - \mu$. This article consists of two parts. In the first part in Sec. II we use Boltzmann theory to calculate the relaxation rate for spin transport in this system for arbitrary interaction strength, both close to the BCS pairing transition and for temperatures much higher than the Fermi temperature. Then, using the noninteracting spin susceptibility, we can determine the spin-diffusion constant using the Einstein relation. This calculation incorporates the effect of pairing fluctuations but does not take into account the pseudogap physics or the effect of the finite lifetime of the quasiparticle eigenstates. At the diagrammatic level, however, this calculation includes vertex corrections.

In the second part in Sec. III we calculate the fermion self-energy at unitarity both close to the BCS pairing transition and for high temperatures within the many-body T-matrix approximation. This self-energy is the many-body T matrix closed with a bare (noninteracting) fermion line. Using this self-energy, we determine the spectral function and the spin-transport relaxation rate and spin susceptibility ignoring vertex corrections. Again, the spin-diffusion constant can be obtained using the Einstein relation. We end in Sec. IV with our conclusions.

By comparing the spin-transport relaxation rate and diffusion constant obtained using both methods, we assess the importance of pseudogap physics, finite lifetime effects, and vertex corrections. We find that although the results of these two methods for the transport coefficients differ quantitatively, there is qualitative agreement. This indicates that pseudogap physics, finite lifetime effects, and vertex corrections do not have a critical influence on the prediction using Boltzmann theory for the behavior of transport coefficients close to the BCS transition.

II. BOLTZMANN THEORY

In this section we derive an expression for the spin-transport relaxation rate using the Boltzmann equation. We incorporate many-body effects, so-called pair correlations, close the BCS pairing transition. We apply a spin-dependent driving force $\boldsymbol{F}_\uparrow = \boldsymbol{F}$ and $\boldsymbol{F}_\downarrow = -\boldsymbol{F}$, which will give rise to a spin current $\boldsymbol{j}_s$. The momentum increase by the driving force is balanced by the momentum relaxation due to the interaction between opposite spins, so that the system reaches a steady state. This mechanism is called spin drag. In linear response, the quantum kinetic equations are written as

$$\frac{1}{\hbar}\boldsymbol{F}\cdot\partial_{\boldsymbol{k}} n_F(\xi(\boldsymbol{k})) = \Gamma_\uparrow(\boldsymbol{k}), \tag{1}$$

$$-\frac{1}{\hbar}\boldsymbol{F}\cdot\partial_{\boldsymbol{k}} n_F(\xi(\boldsymbol{k})) = \Gamma_\downarrow(\boldsymbol{k}), \tag{2}$$

where $n_F(\epsilon) = 1/[1+\exp(\beta\epsilon)]$ is the Fermi-Dirac distribution, with $\beta = 1/k_B T$ being the inverse thermal energy, and where the collision integral $\Gamma_\sigma(\boldsymbol{k})$ gives the net particle flux into the $(\boldsymbol{k},|\sigma\rangle)$ state due to interspecies interactions. The Fermi's golden rule expression for $\Gamma_\uparrow(\boldsymbol{k})$ is

$$\Gamma_\uparrow(\boldsymbol{k}) = \frac{2\pi}{\hbar V^2}\sum_{\boldsymbol{k}_1,\boldsymbol{k}_2,\boldsymbol{k}_3,\boldsymbol{k}_4}\delta_{\boldsymbol{k}_1+\boldsymbol{k}_2,\boldsymbol{k}_3+\boldsymbol{k}_4}\delta(\xi_1+\xi_2-\xi_3-\xi_4) \times |T^{MB}|^2 f_{\uparrow,1} f_{\downarrow,2}(1-f_{\downarrow,3})(1-f_{\uparrow,4})(\delta_{\boldsymbol{k}_1,\boldsymbol{k}}-\delta_{\boldsymbol{k}_4,\boldsymbol{k}}), \tag{3}$$

where V is the volume and where we used a shorthand notation for the energy $\xi_i = \xi(\boldsymbol{k}_i)$ and for the nonequilibrium distributions $f_{\sigma,i} = f_\sigma(\boldsymbol{k}_i)$. We note that an analogous expression holds for $\Gamma_\downarrow(\boldsymbol{k})$. Equation (3) considers the total effect of incoming particles with momenta and spin $\boldsymbol{k}_1$, $\uparrow$ and $\boldsymbol{k}_2$, $\downarrow$ that are scattered into momenta and spin $\boldsymbol{k}_3$, $\downarrow$ and $\boldsymbol{k}_4$, $\uparrow$. Momentum and energy conservation is ensured by the Kronecker δ and Dirac δ, respectively. The many-body T matrix T^{MB} gives the scattering amplitude incorporating the effects of the medium and will be specified below.

The distribution functions are shifted from the equilibrium distribution by a momentum $\boldsymbol{k}_\sigma = m\boldsymbol{v}_\sigma/\hbar$, where $\boldsymbol{v}$ is the so-called drift velocity, which is related to the spin current by $\boldsymbol{j}_s = n_\uparrow \boldsymbol{v}_\uparrow - n_\downarrow \boldsymbol{v}_\downarrow = 2n\boldsymbol{v}$. Here, we used the fact that due to symmetry the drift velocities of the two species will be opposite and of equal magnitude for both species. The distribution function $f_\sigma(\boldsymbol{k})$ to first order in the drift velocity is $f_\sigma(\boldsymbol{k}) = n_F(\xi_\sigma(\boldsymbol{k})) + f^1_\sigma(\boldsymbol{k})$, where $f^1_\sigma(\boldsymbol{k}) = -\hbar(\boldsymbol{v}_\sigma\cdot\boldsymbol{k})n'_F(\xi_\sigma(\boldsymbol{k}))$. By

subtracting Eq. (2) from Eq. (1), multiplying with $\hbar\boldsymbol{k}$, and summing over $\boldsymbol{k}$, we arrive at the momentum balance equation,

$$-n\boldsymbol{F} = \frac{1}{V}\sum_{\boldsymbol{k}}(\hbar\boldsymbol{k})\Gamma(\boldsymbol{k}) = \tilde{\Gamma}\boldsymbol{v} + O(v^2), \tag{4}$$

where the coefficient $\tilde{\Gamma}$ of the linear term in the right-hand side is given by

$$\tilde{\Gamma} = -\frac{\pi\beta\hbar}{6V^3}\sum_{\boldsymbol{k}_i}\delta_{\boldsymbol{k}_1+\boldsymbol{k}_2,\boldsymbol{k}_3+\boldsymbol{k}_4}\delta(\xi_1+\xi_2-\xi_3-\xi_4) \times |T^{MB}|^2 n_1 n_2(1-n_3)(1-n_4)(\boldsymbol{k}_1-\boldsymbol{k}_2+\boldsymbol{k}_3-\boldsymbol{k}_4)^2 \tag{5}$$

and we introduced the shorthand notation $n_i = n_F(\xi(\boldsymbol{k}_i))$. We introduce the spin-drag conductivity σ_D via $\boldsymbol{j}_s = \sigma_D\boldsymbol{F}$ and from Eq. (4) we identify $\sigma_D = -2n^2/\tilde{\Gamma}$. The spin-drag conductivity can be related to the spin-transport relaxation rate $1/\tau_D$ by the Drude formula $\sigma_D = 2n\tau_D/m$, leading to $1/\tau_D = -\tilde{\Gamma}/mn$.

To make further progress, we rewrite Eq. (5) in a form that is convenient to account for a divergence in the pairing channel due to pairing fluctuations close to the superfluid transition. First, we introduce an additional energy integral over the variable $\hbar\omega = \xi(\boldsymbol{k}_1)+\xi(\boldsymbol{k}_2)$, i.e., the sum of the energies of the two incoming particles in the scattering event. This choice is convenient because close to the superfluid transition, in the on-shell approximation, the dominant energy on which T^{MB} depends is $\hbar\omega$. We stress that this choice is different from the conventional one, where $\hbar\omega$ is taken to be the difference between the energies of the incoming and outgoing $\uparrow$ particles [3]. Next, we resolve the momentum-conserving Kronecker delta $\delta_{\boldsymbol{k}_1+\boldsymbol{k}_2,\boldsymbol{k}_3+\boldsymbol{k}_4}$ in Eq. (5) by choosing $\boldsymbol{k}_1 = \boldsymbol{k}+\boldsymbol{K}/2$, $\boldsymbol{k}_2 = \boldsymbol{K}/2-\boldsymbol{k}$, $\boldsymbol{k}_3 = \boldsymbol{k}'+\boldsymbol{K}/2$, and $\boldsymbol{k}_4 = \boldsymbol{K}/2-\boldsymbol{k}'$, and we introduce an additional energy integral via

$$\delta(\xi_1+\xi_2-\xi_3-\xi_4) = \int d(\hbar\omega)\delta(\xi_1+\xi_2-\hbar\omega)\delta(\xi_3+\xi_4-\hbar\omega). \tag{6}$$

Then, after using the Dirac identity $\mathrm{Im}[1/(x+i0)] = -\pi\delta(x)$, we rewrite Eq. (5) into

$$\frac{1}{\tau_D} = \frac{\pi\beta\hbar}{6\pi^2 mn}\int\frac{d\boldsymbol{k}}{(2\pi)^3}\frac{d\boldsymbol{k}'}{(2\pi)^3}\frac{d\boldsymbol{K}}{(2\pi)^3}d(\hbar\omega)(\boldsymbol{k}'+\boldsymbol{k})^2 \times\frac{|T^{MB}(\boldsymbol{K},\hbar\omega)|^2}{\sinh^2(\beta\hbar\omega/2)} \times\mathrm{Im}\left[\frac{1-n_F(\xi(\boldsymbol{k}+\boldsymbol{K}/2))-n_F(\xi(\boldsymbol{K}/2-\boldsymbol{k}))}{\hbar\omega+i0-[\xi(\boldsymbol{k}+\boldsymbol{K}/2)+\xi(\boldsymbol{K}/2-\boldsymbol{k})]}\right] \times\mathrm{Im}\left[\frac{1-n_F(\xi(\boldsymbol{k}'+\boldsymbol{K}/2))-n_F(\xi(\boldsymbol{K}/2-\boldsymbol{k}'))}{\hbar\omega+i0-[\xi(\boldsymbol{k}'+\boldsymbol{K}/2)+\xi(\boldsymbol{K}/2-\boldsymbol{k}')]}\right]. \tag{7}$$

The effective interaction is given by the many-body matrix element $T^{MB}(\boldsymbol{K},\hbar\omega)$, which takes a simple form close to the superfluid transition in these variables:

$$T^{MB}(\boldsymbol{K},\hbar\omega) = \frac{V_0}{1-V_0\Xi(\boldsymbol{K},\hbar\omega)}, \tag{8}$$

where $V_0 = 4\pi a\hbar^2/m$, with a being the s-wave scattering length. The bare pairing susceptibility Ξ is given by

$$\Xi(\boldsymbol{K},\hbar\omega) = \frac{1}{V}\sum_{\boldsymbol{k}}\left[\frac{1-n_F(\xi(\boldsymbol{k}+\boldsymbol{K}/2))-n_F(\xi(\boldsymbol{k}-\boldsymbol{K}/2))}{\hbar\omega+i0-[\xi(\boldsymbol{k}+\boldsymbol{K}/2)+\xi(\boldsymbol{k}-\boldsymbol{K}/2)]} + \frac{1}{2\epsilon(\boldsymbol{k})}\right], \tag{9}$$

with $\epsilon(\boldsymbol{k}) = \hbar^2k^2/2m$. The second term of the summand cures the ultraviolet divergence of summing the first term. Its derivation can be found in Ref. [19]. We note that the transition temperature T_c to the superfluid state is determined by $1/T^{MB}(\boldsymbol{0},0) = 0$. In Eq. (7), we can perform the integrals over $\boldsymbol{k}$, $\boldsymbol{k}'$, and the angles of $\boldsymbol{K}$ exactly. The integrals over ω and the length of $\boldsymbol{K}$ must then be performed numerically. Our theory does not take into account the superfluid gap or the presence of Cooper pairs for $T < T_c$ and is thus only valid for temperature higher than the transition temperature.

To obtain results for $1/\tau_D$ at constant density, we need to solve the noninteracting equation of state $n = (1/V)\sum_{\boldsymbol{k}} n_F(\xi(\boldsymbol{k}))$, which yields the function $\mu(T,n)$. For low temperatures, μ is given by the familiar relation $\mu = \epsilon_F[1-(\pi^2/12)(k_BT/\epsilon_F)^2]$. Here, the Fermi energy $\epsilon_F = k_BT_F = \hbar^2k_F^2/2m$, with the Fermi wave number $k_F = (6\pi^2n)^{1/3}$. The transition temperature can then be determined as a function of the dimensionless interaction parameter k_Fa. We find at unitarity ($-1/k_Fa = 0$) $T_c \approx 0.50T_F$ and that for weak coupling (where $-1/k_Fa \gg 1$) $T_c \propto T_F\exp(-\pi/2k_F|a|)$. In Fig. 1 we show the dimensionless spin-transport relaxation rate $\hbar/\epsilon_F\tau_D$ obtained from Eq. (7) as a function of the reduced temperature T/T_F. Each curve terminates at the value of the transition temperature corresponding to its k_Fa value. These curves illustrate a number of effects. First, we see that, for all k_Fa, the relaxation rate is enhanced (but remains finite) when approaching T_c from above. This enhancement is larger in the strong-coupling case than in the weak-coupling case. The reason for this enhancement is that pairing fluctuations become important close to the superfluid transition, which leads to the

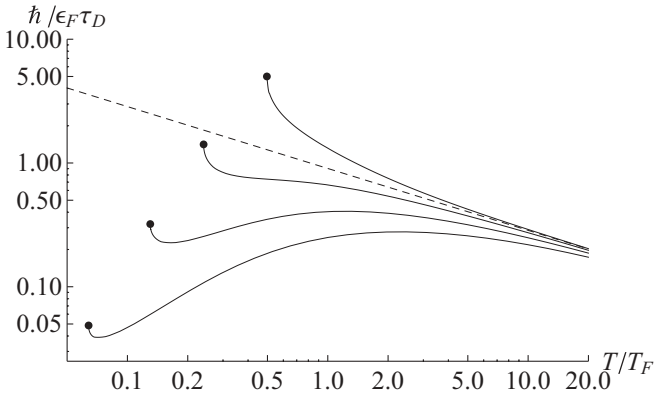

FIG. 1. The dimensionless spin-transport relaxation rate $\hbar/\epsilon_F\tau_D$ obtained from Eq. (7) as a function of the reduced temperature T/T_F. From top to bottom the curves correspond to interaction parameters $-1/k_Fa = \{0, 0.56, 1.0, 1.4\}$. Each curve terminates at the value of the transition temperature corresponding to its k_Fa value: in decreasing order these are $T/T_F \approx \{0.50, 0.24, 0.13, 0.064\}$. The dashed line is the high-temperature asymptote $1/\tau_D \propto 1/\sqrt{T}$ predicted in Ref. [6].

appearance of a pole in T^{MB} in the integrand of Eq. (7) at $\boldsymbol{K} = \boldsymbol{0}$ and $\omega = 0$.

For large temperatures, all curves approach the dashed line in Fig. 1 given by $1/\tau_D = (\epsilon_F/\hbar)(32\sqrt{2}/9\pi^{3/2})\sqrt{T_F/T}$, which falls off as $1/\sqrt{T}$ and was determined in [6]. The $1/\sqrt{T}$ dependence can be understood by noting that $1/\tau \propto n v \sigma$, where n is the density, v is the mean particle velocity, and σ is the cross section at unitarity. For temperatures $T \gg T_F$, the scattering cross section is given by the square of the thermal de Broglie wavelength, and thus σ decreases like $1/T$. Since for high temperatures it holds that $v \propto \sqrt{T}$, we find $1/\tau \propto 1/\sqrt{T}$. This high-temperature behavior was also measured experimentally [4].

In the weak-coupling case ($-1/k_F a \gtrsim 1$), we note an increase of $1/\tau_D$ with temperature up to $T \approx T_F$. An increase in temperature leads to a larger phase space being available for scattering events due to reduced Pauli blocking. In the absence of many-body effects ($T^{MB} = V_0$), this effect would lead to the standard T^2 dependence of transport coefficients in a Fermi liquid. Indeed, when $T^{MB} = V_0$, we recover the weak-coupling result by Bruun, $1/\tau_D = (16\pi/9)(k_F^2 a^2 \epsilon_F/\hbar)(T/T_F)^2$ for $T \ll T_c$ [6].

We note that our theory overestimates T_c at unitarity in comparison with the value $T_c = 0.15 T_F$ obtained by Monte Carlo and renormalization group methods (see, e.g., Ref. [20]). In this sense, the experimental result for the spin-transport relaxation rate in Ref. [4] should not be compared to the top curve in Fig. 1 at unitarity but instead to the second one from the bottom, which has a finite $k_F a$ value and $T_c = 0.13 T_F$. Then, we see that our result agrees qualitatively with the experimental results in Ref. [4].

To obtain the diffusion constant D_s we use the Einstein relation $D_s = \sigma_D/\chi_s$. For the spin susceptibility, we use the noninteracting result $\chi_s = -(1/V)\sum_k n'(\xi(\boldsymbol{k}))$. The result is shown in Fig. 2, where we plot the diffusion constant scaled by $m/\hbar$ versus the reduced temperature. The vertical order of the curves is reversed with respect to Fig. 1. Each curve again terminates at the value of the transition temperature corresponding to its $k_F a$ value. The remarks made about Fig. 1 largely carry over to our results for the diffusion constant in Fig. 2. We see a suppression of D_s when approaching the transition for all $k_F a$ values. For the top two curves with $-1/k_F a = \{1.0, 1.4\}$ we see that the nonmonotonic behavior of $1/\tau_D$ is also present in the curves for D_s, which for these $k_F a$ values now have a minimum around $T/T_F = 0.5$. Since χ_s follows the Curie law $\chi_s = n/k_B T$ for high temperatures, we find that for high temperatures $D_s = (\hbar/m)(9\pi^{3/2}/16\sqrt{2})(T/T_F)^{3/2}$, which is shown as the dashed line in Fig. 2. We note the factor of 2 difference with the result for this asymptote from Ref. [6], which is caused by a different definition of σ_D. We note that if we again compare the second curve from the top, which has a finite $k_F a$ value and $T_c = 0.13 T_F$, with the experimental results from Ref. [4] at unitarity, we see qualitative agreement: both curves flatten off for temperatures below $T/T_F = 0.5$. Considering our results, we see that this behavior is actually the crossover behavior between the monotonic behavior of the unitary (bottom) curve in Fig. 2 and the nonmonotonic behavior of the weak-coupling (top) curve. Clearly, a strength of our approach is that we can determine the whole temperature range using a single approach.

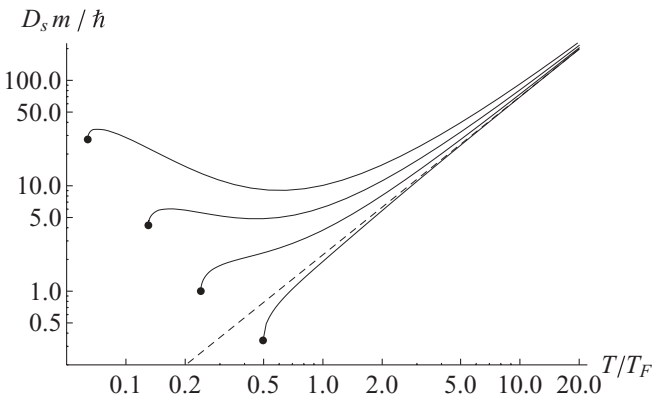

FIG. 2. The dimensionless spin-diffusion constant $D_s m/\hbar$ obtained from the result of Fig. 1 using the Einstein relation. From bottom to top the curves correspond to interaction parameters $-1/k_F a = \{0, 0.56, 1.0, 1.4\}$. Each curve terminates at the value of the transition temperature corresponding to its $k_F a$ value. The dashed line is the high-temperature asymptote $D_s = (\hbar/m)(9\pi^{3/2}/16\sqrt{2})(T/T_F)^{3/2}$.

III. DIAGRAMMATIC THEORY

In the second part of this work, we use a diagrammatic approach to determine the self-energy, spectral functions, and transport coefficients.

A. Definitions

First, we recall some aspects of the microscopic theory of an interacting gas of fermions. The central quantity in this theory is the self-energy, which is the sum of all one-particle reducible diagrams, and the spectral function derived from it. For reference we give the expressions for the spectral function and the density of states and the particle density in an interacting system in terms of the spectral function. For a system which is translationally invariant in space and time, the retarded fermion Green's function is given by

$$G(\boldsymbol{k},\omega) = \frac{-\hbar}{-\hbar\omega^+ + \xi(\boldsymbol{k}) + \hbar\Sigma(\boldsymbol{k},\omega)}, \tag{10}$$

where $\Sigma(\boldsymbol{k},\omega)$ is the retarded self-energy. The spectral function describes the weight of a single-particle excitation and is given by

$$\begin{aligned}\rho(\boldsymbol{k},\omega) &= -\frac{1}{\pi\hbar}\mathrm{Im}[G(\boldsymbol{k},\omega)] \\ &= -\frac{1}{\pi\hbar}\frac{\mathrm{Im}\Sigma(\boldsymbol{k},\omega)}{[-\omega + \xi(\boldsymbol{k})/\hbar + \mathrm{Re}\Sigma(\boldsymbol{k},\omega)]^2 + \mathrm{Im}^2\Sigma(\boldsymbol{k},\omega)}.\end{aligned} \tag{11}$$

In the absence of interactions, $\Sigma = 0$ and the spectral function is a δ peak at $\hbar\omega = \xi(\boldsymbol{k})$. A nonzero real part of Σ will shift the δ peak to the solution of $\omega = \xi(\boldsymbol{k})/\hbar + \mathrm{Re}\Sigma(\boldsymbol{k},\omega)$, while a nonzero $\mathrm{Im}\Sigma$ will lead to a broadening of the peak, indicating a finite lifetime of the single-particle excitation. In particular, a constant $\mathrm{Im}\Sigma = -1/2\tau$ will lead to a spectral function with a Lorentzian shape with width τ. We note several relations for

the spectral function that we use later. The sum rule states that

$$\int d(\hbar\omega)\rho(\boldsymbol{k},\omega) = 1, \tag{12}$$

and it follows from the anticommutation relation of the fermion fields. The density of states is

$$\nu(\omega) = \frac{1}{(2\pi)^3}\int d\boldsymbol{k}\rho(\boldsymbol{k},\omega), \tag{13}$$

and the equation of state is

$$n = \int d(\hbar\omega)n_F(\omega)\nu(\omega). \tag{14}$$

Using the Kubo formalism, we obtain the spin-transport relaxation rate $1/\tau_D$ and spin susceptibility $\chi_s = \partial(n_\uparrow - n_\downarrow)/\partial(\mu_\uparrow - \mu_\downarrow)$ in terms of the spectral function. These are in the absence of vertex corrections given by

$$\frac{1}{\tau_D} = -\frac{3mn}{\pi\hbar^3}\left[\frac{1}{V}\sum_{\boldsymbol{k}}\boldsymbol{k}^2\int d(\hbar\omega)\rho^2(\boldsymbol{k},\omega)n'(\hbar\omega)\right]^{-1} \tag{15}$$

and

$$\chi_s = -\frac{1}{V}\sum_{\boldsymbol{k}}\int d(\hbar\omega)d(\hbar\omega') \times \rho(\boldsymbol{k},\omega)\rho(\boldsymbol{k},\omega')\frac{n_F(\hbar\omega) - n_F(\hbar\omega')}{\hbar\omega - \hbar\omega'}. \tag{16}$$

We note that Eq. (15) can be derived by calculating the ordinary Drude conductivity of the atoms with spin up, say, in the presence of scattering from an "external" potential which is due to the presence of atoms with spin down. We note that for $\Sigma = -i/2\tau$, Eq. (15) gives $1/\tau_D = 1/\tau$ and that in the noninteracting case for low temperatures, Eq. (16) reduces to the well-known $\chi_0 = 3n/2\epsilon_F$. Finally, we note that we can obtain the spin-diffusion constant D_s via the Einstein relation $D_s = \sigma_D/\chi_s$.

B. Self-energy

We calculate the fermion self-energy which is appropriate for this system both close to the BCS pairing transition and for high temperatures at unitarity [21]. Indeed, the many-body T matrix closed with a noninteracting fermion line, shown in Fig. 3, incorporates the effect of enhancement of the interaction close to the BCS transition. In the dilute limit for weak interactions, where $T^{MB} \to V_0$, it reduces to the standard mean-field shift of the dispersion $V_0 n$. The expression for Σ as a function of momentum $\boldsymbol{k}$ and fermionic Matsubara frequency ω_n is

$$\Sigma(\boldsymbol{k},i\omega_n) = \frac{1}{\hbar^2\beta}\frac{1}{V}\sum_{\boldsymbol{K},\omega_m} T^{MB}(\boldsymbol{K},i\hbar\omega_m) \times G_0(\boldsymbol{K}-\boldsymbol{k},i\hbar(\omega_m - \omega_n)), \tag{17}$$

where the summation is over the bosonic Matsubara frequencies ω_m, G_0 is the noninteracting Green's function, and $T^{MB}(\boldsymbol{K},i\hbar\omega_m)$ denotes the many-body T matrix [Eq. (8)]. We compute the Matsubara summation of Eq. (17) to obtain

$$\mathrm{Im}\Sigma(\boldsymbol{k},\omega) = \frac{1}{\hbar}\frac{1}{V}\sum_{\boldsymbol{K}}[n_F(\xi(\boldsymbol{K}-\boldsymbol{k})) + n_b(\xi(\boldsymbol{K}-\boldsymbol{k}) + \hbar\omega)] \times \mathrm{Im}[T^{MB}(\boldsymbol{K},\xi(\boldsymbol{K}-\boldsymbol{k}) + \hbar\omega)]. \tag{18}$$

Using $\mathrm{Im}[T^{MB}(\boldsymbol{K},\hbar\omega)] = \mathrm{Im}[\Xi(\boldsymbol{K},\hbar\omega)]|T^{MB}(\boldsymbol{K},\hbar\omega)|^2$, we can rewrite Eq. (18) as

$$\mathrm{Im}\Sigma(\boldsymbol{k},\omega) = -\frac{\pi}{\hbar V^2}\sum_{\boldsymbol{k}_2,\boldsymbol{k}_3,\boldsymbol{k}_4}\delta(\hbar\omega + \xi(\boldsymbol{k}_2) - \xi(\boldsymbol{k}_3) - \xi(\boldsymbol{k}_4)) \times \delta_{\boldsymbol{k}+\boldsymbol{k}_2,\boldsymbol{k}_3+\boldsymbol{k}_4}|T^{MB}(\boldsymbol{k}+\boldsymbol{k}_2,\hbar\omega + \xi(\boldsymbol{k}_2))|^2 \times [n_2(1-n_3)(1-n_4) + (1-n_2)n_3n_4], \tag{19}$$

where we again used the shorthand notation $n_i = n_F(\xi(\boldsymbol{k}_i))$. Since $\mathrm{Im}\Sigma$ is a single-particle relaxation rate, we see that this rate is exactly the sum of the in and out rates for the state with momentum $\boldsymbol{k}$ and energy $\hbar\omega$, as would be obtained from a Fermi's golden-rule expression. In Eq. (19), we introduce the center-of-mass momentum $\boldsymbol{K} = \boldsymbol{k} + \boldsymbol{k}_2$ and an additional energy integral

$$\delta(\hbar\omega + \xi(\boldsymbol{k}_2) - \xi(\boldsymbol{k}_3) - \xi(\boldsymbol{k}_4)) = \int d(\hbar\Omega)\delta(\hbar\omega + \xi(\boldsymbol{k}_2) - \hbar\Omega)\delta(\xi(\boldsymbol{k}_3) + \xi(\boldsymbol{k}_4) - \hbar\Omega). \tag{20}$$

After some rewriting, we then arrive at the following expression for $\mathrm{Im}\Sigma$:

$$n_F(\omega)[1-n_F(\omega)]\mathrm{Im}\Sigma(\boldsymbol{k},\hbar\omega) = \frac{m}{8\pi^2 k\hbar^3}\int_R d(\hbar\Omega)dK\frac{|T^{MB}(K,\hbar\Omega)|^2}{\sinh^2(\beta\hbar\Omega/2)}\mathrm{Im}[\Xi(K,\hbar\Omega)] \times [1 - n_F(\hbar\Omega - \hbar\omega) - n_F(\hbar\omega)], \tag{21}$$

which is a convenient starting point for numerical evaluation. In going from Eqs. (19) to (21), we introduced $\mathrm{Im}\Xi$ from Eq. (9). The δ functions on the right-hand side of Eq. (20) restrict the integration range to R, which is defined by the following inequalities:

$$2\mu + \hbar\omega - \tfrac{1}{2}\epsilon(K) > 0, \qquad \mu + \hbar\Omega - \hbar\omega > 0, \tag{22}$$

and

$$|\sqrt{\epsilon(k)} - \sqrt{\mu + \hbar\Omega - \hbar\omega}| < \sqrt{\epsilon(K)} < \sqrt{\epsilon(k)} + \sqrt{\mu + \hbar\Omega - \hbar\omega}, \tag{23}$$

where we defined $\epsilon(k) = \hbar^2k^2/2m$. Then, the real part of the self-energy is obtained by a Kramers-Kronig transform,

$$\mathrm{Re}\Sigma(\boldsymbol{k},\omega) = \frac{1}{\pi}\int d\omega'\frac{\mathrm{Im}\Sigma(\boldsymbol{k},\hbar\omega)}{\omega' - \omega}. \tag{24}$$

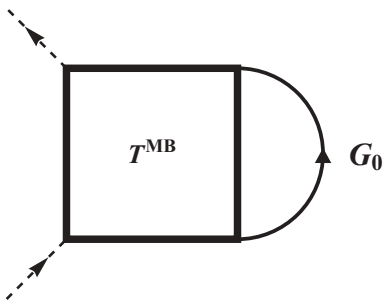

FIG. 3. The self-energy Σ is the many-body T matrix closed with a single noninteracting Green's-function line. The external lines are indicated by the dashed lines.

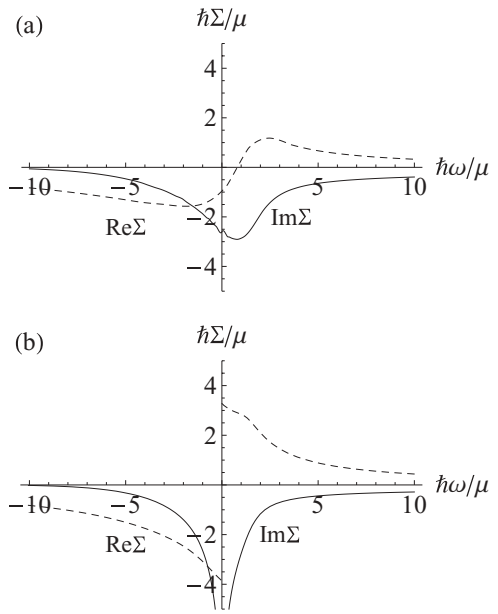

FIG. 4. The imaginary (solid line) and real (dashed line) parts of the self-energy at unitarity for $\hbar k = \sqrt{2m\mu}$ for (a) $k_B T/\mu = 1$ and (b) $T = T_c$.

In the next section, we show the results for the spectral function and spin-transport coefficients obtained by evaluating Eqs. (21) and (24).

C. Results

In the simplest approximation the spin-drag relaxation rate is determined by the imaginary part of the self-energy at the Fermi energy and Fermi momentum. Hence, we first determine the self-energy. By evaluating Eqs. (21) and (24) numerically, we obtain Fig. 4, where we show the imaginary (solid line) and real (dashed line) parts of the self-energy for the momentum $\hbar k = \sqrt{2m\mu}$ at unitarity (see also Ref. [16]). Figure 4(a) shows the results far from the transition at $T = \mu/k_B \approx 1.5T_c$, and Fig. 4(b) shows the results at the transition $T = T_c$. From Fig. 4 we see that upon approaching the transition, a divergence develops at $\omega = 0$ in the imaginary part of the self-energy and a corresponding discontinuity develops in the real part. Closer inspection shows that the imaginary part diverges logarithmically. When $\mathrm{Im}\Sigma$ diverges as $x \ln(\Delta\omega)$, with $\Delta\omega$ being the distance from the pole, the resulting jump in the real part is πx. For general $\boldsymbol{k}$, the position of the divergence is $\hbar\omega = -\xi(\boldsymbol{k})$, which can be understood as follows: the transition is accompanied by a pole in the many-body T matrix $T^{MB}(\boldsymbol{K},\hbar\Omega)$ for $\boldsymbol{K} = \boldsymbol{0}$ and $\hbar\Omega = 0$. In the expression for $\mathrm{Im}\Sigma$ [Eq. (19)] the T matrix enters as $T^{MB}(\boldsymbol{k}+\boldsymbol{k}_2,\hbar\omega+\xi(\boldsymbol{k}_2))$, so that for $\hbar\omega = -\xi(\boldsymbol{k})$, the conditions $\boldsymbol{K} = \boldsymbol{0}$ and $\hbar\Omega = 0$ are satisfied when $\boldsymbol{k}_2 = -\boldsymbol{k}$.

As a check, we may also obtain the logarithmic divergence analytically. The divergence is caused by the development of a pole at $\Omega = 0$ and $K = 0$ in Eq. (21). For small Ω and K, $T^{MB} \propto 1/[a_1\Omega + a_2K^2 + a_3(T - T_c) + ia_4\Omega]$ (with a_i being real) while the rest of the integrand is linear in K. Integration over Ω and K then yields a divergence $\ln(T - T_c)$. In contrast, for small Ω and K the integrand in the Boltzmann case [Eq. (7)] goes as K^2. Integration shows that there is then no divergence, as was shown in Fig. 1.

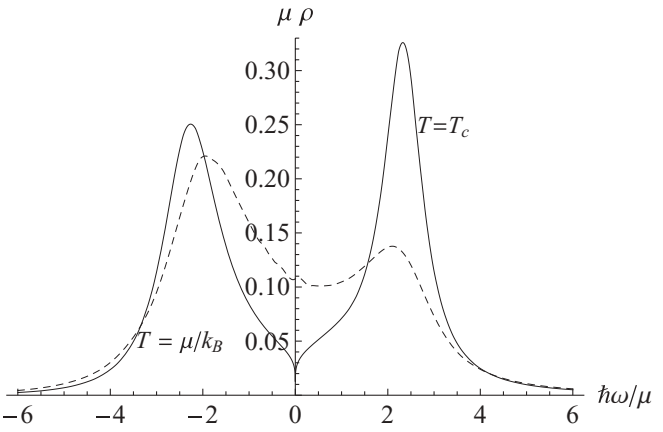

FIG. 5. The spectral function ρ at unitarity for $\hbar k = \sqrt{2m\mu}$ for $k_B T/\mu = 1$ (dashed line) and $T = T_c$ (solid line).

From Eq. (11) we see that a divergence of $\mathrm{Im}\Sigma$ will lead to a suppression of the spectral function ρ. Indeed, in Fig. 5 we show the spectral function ρ at unitarity for $\hbar k = \sqrt{2m\mu}$ for $k_B T/\mu = 1$ (dashed line) and $T = T_c$ (solid line). Already, quite far from the transition at $T = \mu/k_B \approx 1.5T_c$, interactions cause a suppression of the spectral weight close to $\omega = 0$, which moves into peaks on both sides of $\omega = 0$ in order to keep the sum rule satisfied. At $T = T_c$, this suppression is maximal, and here ρ vanishes logarithmically as $|\omega| \to 0$. We note, however, that the suppression of the spectral weight occurs at lower temperatures when considering the spectral function at $k = k_F$ [16].

In Fig. 6 we show the solution of the equation of state $n = \int d(\hbar\omega) n_F(\omega)\nu(\omega)$ for μ. The dashed line corresponds to the noninteracting result, which was used to obtain the Boltzmann results in Fig. 1. The solid line is the solution of the number equation at unitarity, which terminates at the critical temperature $T_c \approx 0.29T_F$. The difference of this value for T_c from the mean-field value for T_c at unitarity $T_c \approx 0.5T_F$ used in Sec. II is that there we used the noninteracting equation of state. That μ is lower than the noninteracting value is intuitively clear: an attractive interaction will lower the energy of the

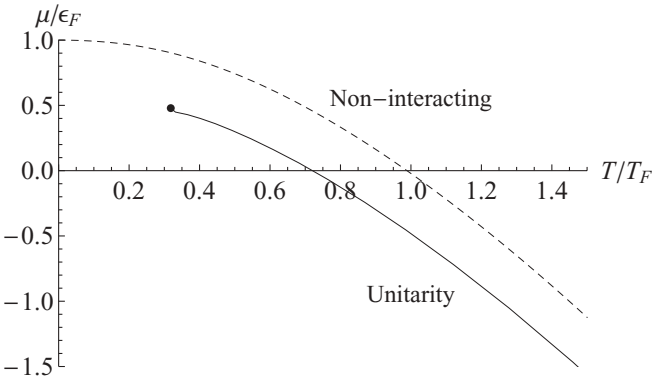

FIG. 6. The solution of the number equation giving μ as a function of temperature. The dashed line is the noninteracting result. The solid line gives the result at unitarity.

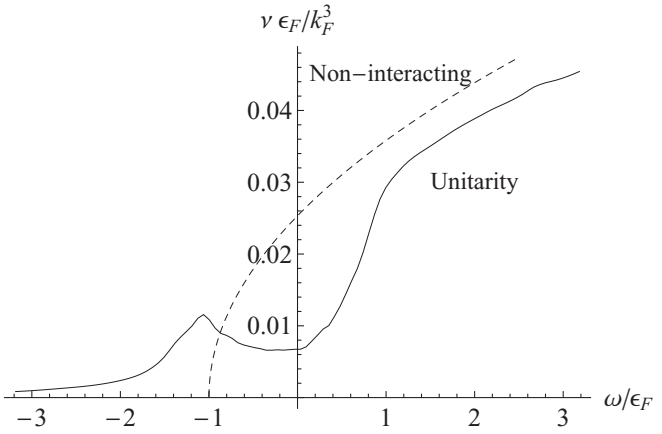

FIG. 7. The density of states ν vs ω. The dashed curve is the noninteracting result for $T = 0$, while the solid curve corresponds to the unitary case for $T = T_c$.

atoms, and thus μ must also be lowered in order to keep the number of particles the same.

In Fig. 7 we show the density of states ν versus ω. The dashed curve is the noninteracting result at $T = 0$, which goes as $\nu \propto \sqrt{\omega - \epsilon_F}$. The solid curve is the result at unitarity at $T = T_c$. We see that the suppressed spectral weight around $\omega = 0$ leads to a greatly reduced density of states, a so-called pseudogap. We note that since T_c is not particularly low, the spectral functions are never very sharply peaked, and the density of states remains nonzero in the pseudogap, in agreement with the results of Ref. [16].

In Fig. 8 we show the spin-transport relaxation rate obtained by evaluating Eq. (15) at unitarity as a solid line. The dashed line is the unitarity result from the Boltzmann calculation (the top line in Fig. 1). Since both lines are determined using different equations of state, they terminate at different T_c. Similarly, in Fig. 9 we show the spin-diffusion constant. The dashed line is the unitarity result from the Boltzmann calculation (the bottom line in Fig. 2), while the solid line is obtained by evaluating the spin susceptibility in Eq. (16) and using the Einstein relation to find D_s.

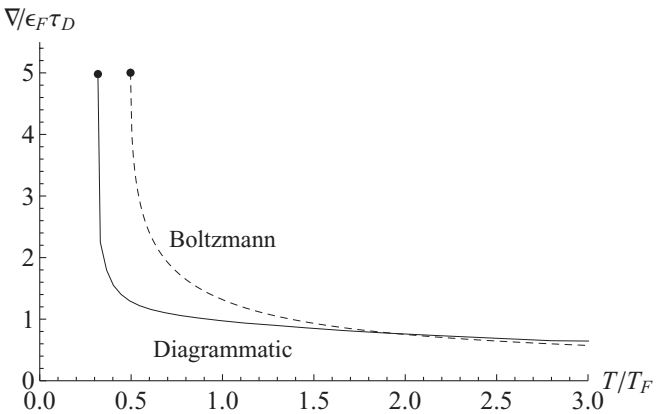

FIG. 8. The spin-transport relaxation rate $1/\tau_D$ as a function of temperature at unitarity. The dashed line is the Boltzmann result, and the solid line is the diagrammatic result obtained by evaluating Eq. (15).

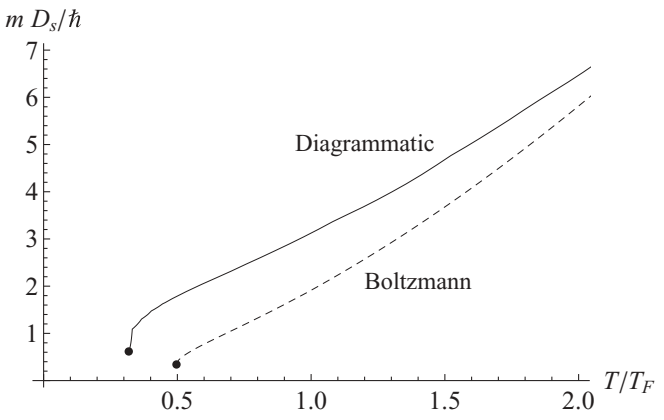

FIG. 9. The spin-diffusion constant D_s as a function of temperature at unitarity. The dashed line is the Boltzmann result, and the solid line is the diagrammatic result obtained by evaluating the spin susceptibility in Eq. (16) and using the Einstein relation.

In Fig. 10 we show the spin susceptibility χ_s obtained by evaluating Eq. (16) scaled by the noninteracting zero-temperature value $\chi_0 = 3n/2\epsilon_F$ as a solid line. The dashed line corresponds to the noninteracting result. We see that for large temperatures the lines converge and that our result shows a downturn close to T_c. This downturn is expected physically since the magnetic response should diminish when $\uparrow$ and $\downarrow$ spins become more correlated. The inclusion of Maki-Thompson vertex correction leads to a further suppression of the susceptibility of the spin susceptibility [17]. For a detailed comparison between theory and experiment regarding the spin susceptibility, we also refer to Ref. [17]. We note that in BCS theory (without fluctuations) the downturn of the spin susceptibility happens below T_c.

IV. CONCLUSIONS AND DISCUSSION

We have determined the spin-diffusion constant and the spin-transport relaxation rate using a Boltzmann approach and a diagrammatic approach at unitarity, as shown in Figs. 8 and 9. On a diagrammatic level, the Boltzmann calculation takes into

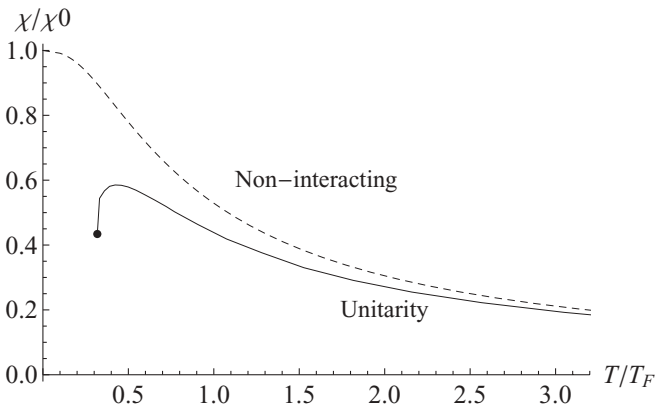

FIG. 10. The spin susceptibility obtained by evaluating Eq. (16) scaled by the noninteracting zero-temperature value $\chi_0 = 3n/2\epsilon_F$ as the solid line. The dashed line corresponds to the noninteracting result. The solid curve terminates at the critical temperature $T_c = 0.29T_F$.

account vertex corrections, while our diagrammatic approach does not. Conversely, the diagrammatic approach takes into account pseudogap physics which suppresses the spectral weight close to the Fermi level, while the Boltzmann approach does not. Surprisingly, we find qualitatively equivalent behavior for both transport coefficients using these approaches. Apparently, pseudogap physics and vertex corrections are not of critical importance when evaluating these transport coefficients close to the BCS transition. [We note, however, that if we would use the approximation $1/\tau_D \propto \mathrm{Im}\Sigma(k_F,\epsilon_F)$, we would find that the spin-drag rate would diverge.] To research this claim further, vertex corrections appropriate to the self-energy we used should be evaluated. For the static spin susceptibility we find our results to be in qualitative agreement with those of Ref. [17], which include both self-energy and vertex corrections. In particular, while the vertex correction is found to significantly reduce the spin susceptibility, a sharp downturn is still clearly observed as the critical temperature is approached from above. In contrast to this, no downturn in the spin susceptibility and no upturn in the spin-drag rate have been found in a recent work [22] in which the Luttinger-Ward theory is used to study spin diffusion in Fermi gases.

In comparing our results to the work of Sommer *et al.* [4], we note that there is some amount of qualitative agreement. One interesting direction for experimental research would be to explore suppression of the spin-drag rate in the Fermi-liquid regime more quantitatively by going to weaker interactions.

ACKNOWLEDGMENTS

This work was supported by the Stichting voor Fundamenteel Onderzoek der Materie (FOM), the Netherlands Organization for Scientific Research (NWO), and the European Research Council (ERC). G.V. was supported by NSF Grant No. DMR -1104788. M.P. was supported by the Italian Ministry of Education, University, and Research (MIUR) through the program "FIRB–Futuro in Ricerca 2010," Project PLASMOGRAPH (Grant No. RBFR10M5BT).

[1] C. P. Weber, N. Gedik, J. E. Moore, J. Orenstein, J. Stephens, and D. D. Awschalom, Nature (London) **437**, 1330 (2005); I. D'Amico and G. Vignale, Phys. Rev. B **62**, 4853 (2000).
[2] T. J. Gramila, J. P. Eisenstein, A. H. MacDonald, L. N. Pfeiffer, and K. W. West, Phys. Rev. Lett. **66**, 1216 (1991).
[3] A. G. Rojo, J. Phys. Condens. Matter **11**, R31 (1999).
[4] A. Sommer, M. Ku, G. Roati, and M. W. Zwierlein, Nature (London) **472**, 201 (2011).
[5] E. Taylor, S. Zhang, W. Schneider, and M. Randeria, Phys. Rev. A **84**, 063622 (2011).
[6] G. M. Bruun, New J. Phys. **13**, 035005 (2011).
[7] S. Hoinka, M. Lingham, M. Delehaye, and C. J. Vale, Phys. Rev. Lett. **109**, 050403 (2012).
[8] R. A. Duine, M. Polini, H. T. C. Stoof, and G. Vignale, Phys. Rev. Lett. **104**, 220403 (2010); R. A. Duine, M. Polini, A. Raoux, H. T. C. Stoof, and G. Vignale, New J. Phys. **13**, 045010 (2011).
[9] H. J. van Driel, R. A. Duine, and H. T. C. Stoof, Phys. Rev. Lett. **105**, 155301 (2010).
[10] S. B. Koller, A. Groot, P. C. Bons, R. A. Duine, H. T. C. Stoof, and P. van der Straten, arXiv:1204.6143.
[11] S. Riedl, E. R. Sánchez Guajardo, C. Kohstall, A. Altmeyer, M. J. Wright, J. H. Denschlag, R. Grimm, G. M. Bruun, and H. Smith, Phys. Rev. A **78**, 053609 (2008).
[12] G. M. Bruun and H. Smith, Phys. Rev. A **72**, 043605 (2005).
[13] B. Y.-K. Hu, Phys. Rev. Lett. **85**, 820 (2000).
[14] A. F. Croxall, K. Das Gupta, C. A. Nicoll, M. Thangaraj, H. E. Beere, I. Farrer, D. A. Ritchie, and M. Pepper, Phys. Rev. Lett. **101**, 246801 (2008); J. A. Seamons, C. P. Morath, J. L. Reno, and M. P. Lilly, *ibid.* **102**, 026804 (2009).
[15] B. Seradjeh, J. E. Moore, and M. Franz, Phys. Rev. Lett. **103**, 066402 (2009); M. P. Mink, H. T. C. Stoof, R. A. Duine, M. Polini, and G. Vignale, *ibid.* **108**, 186402 (2012).
[16] P. Pieri, L. Pisani, and G. C. Strinati, Phys. Rev. Lett. **92**, 110401 (2004); G. M. Bruun and G. Baym, Phys. Rev. A **74**, 033623 (2006); A. Perali, F. Palestini, P. Pieri, G. C. Strinati, J. T. Stewart, J. P. Gaebler, T. E. Drake, and D. S. Jin, Phys. Rev. Lett. **106**, 060402 (2011); C.-C. Chien, H. Guo, Y. He, and K. Levin, Phys. Rev. A **81**, 023622 (2010), and references therein.
[17] F. Palestini, P. Pieri, and G. C. Strinati, Phys. Rev. Lett. **108**, 080401 (2012).
[18] A. Recati and S. Stringari, Phys. Rev. Lett. **106**, 080402 (2011).
[19] H. T. C. Stoof, M. Bijlsma, and M. Houbiers, J. Res. Natl. Inst. Stand. Technol. **101**, 443 (1996).
[20] K. B. Gubbels and H. T. C. Stoof, Phys. Rev. Lett. **100**, 140407 (2008).
[21] S. Fujimoto, J. Phys. Soc. Jpn. **71**, 1230 (2002).
[22] T. Enss and R. Haussmann, Phys. Rev. Lett. **109**, 195303 (2012).